ACS EARTH AND SPACE CHEMISTRY

http://pubs.acs.org/journal/aesccq

Article

Aircraft Measurements from a U.S. Western Wildfire Demonstrating Day and Night Differences in the Chemical Composition and Optical Properties of Biomass Burning Aerosols and Their Atmospheric Evolution

Published as part of ACS Earth and Space Chemistry special issue "Hartmut Hermann Festschrift".

Felipe A. Rivera-Adorno, Lisa Azzarello, Michael A. Robinson, Zachary C. J. Decker, Rebecca A. Washenfelder, Katherine Hayden, Alessandro Franchin, Christopher D. Holmes, Cora J. Young, Carley D. Fredrickson, Brett Palm, Chris Schmidt, Amber Soja, Emily Gargulinski, Steven S. Brown, Ann M. Middlebrook, and Alexander Laskin*

Cite This: https://doi.org/10.1021/acsearthspacechem.4c00215

Read Online

ACCESS | Metrics & More | Article Recommendations | Supporting Information

ABSTRACT: The composition and transformations of biomass burning aerosols (BBA) have been measured onboard the NOAA Twin Otter research aircraft during the Fire Influence on Regional to Global Environments and Air Quality field study. We analyze real-time aerosol mass spectrometry measurements across three flights during the afternoon, late afternoon, and night of August 28, 2019, for one midsized wildfire. Analysis of several metrics showed that the aerosol composition and optical properties varied depending on the burning conditions at the fire zone and the time of day the BBA was emitted, with substantial variations in the available sunlight. The total aerosol mass loadings were dominated by organic components with a much smaller contribution from inorganic species. A gradual buildup of organic material was observed during the afternoon as the plume aged, indicating the condensation of photochemically formed low-volatility oxidized organic compounds. Highly hygroscopic ammonium nitrate was the main inorganic component, suggesting potential water content in BBA particles and the likelihood of their aqueous-phase reactivity. Depletions of particle-phase NO_3^- and Cl^- relative to carbon monoxide were observed in the late afternoon and nighttime plumes, respectively, aligning with known gas-particle partitioning thermodynamics and the heterogeneous chemistry of dissolved nitrate and chloride. The wavelength-dependent light absorption by aerosol species was higher for the plume sampled at night and showed no significant changes with plume age, despite observed trends in composition and mass downwind. These differences in particle composition and optical properties demonstrate that the processes involved in BBA aging are not uniform for the same wildfire over the course of the day and depend highly on when the BBA was emitted, as well as the burning phase at the emissions source.

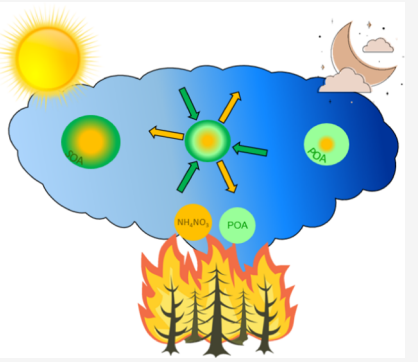

KEYWORDS: *aerosol mass spectrometry, chemical ionization mass spectrometry, particle-into-liquid sampler, real-time chemical analysis, aerosol aging*

INTRODUCTION

Biomass burning aerosols (BBA) emitted from forest fires and prescribed burning events affect Earth's climate directly by absorbing and scattering solar radiation,[1] and indirectly by altering the microphysical properties and lifecycle of clouds.[2−5] Additionally, they have significant impacts on air quality and public health.[6−13] Because of their high chemical complexity, accurately characterizing the properties and impact of BBA remains challenging. Biomass burning events yield a diverse mixture of multicomponent aerosols distributed across the accumulation (<1 μm diameter) and coarse (1−5 μm) modes. Chemically, BBA are predominantly composed of organic and black carbon (i.e., soot), with additional contributions from secondary formed sulfates and nitrates.[14] Primary inorganic components of biomass and surface dust propelled by fire-generated winds also contribute to BBA.[15] The mass fractions and mixing state of BBA individual particles vary between fire

Received: July 30, 2024
Revised: December 12, 2024
Accepted: December 13, 2024

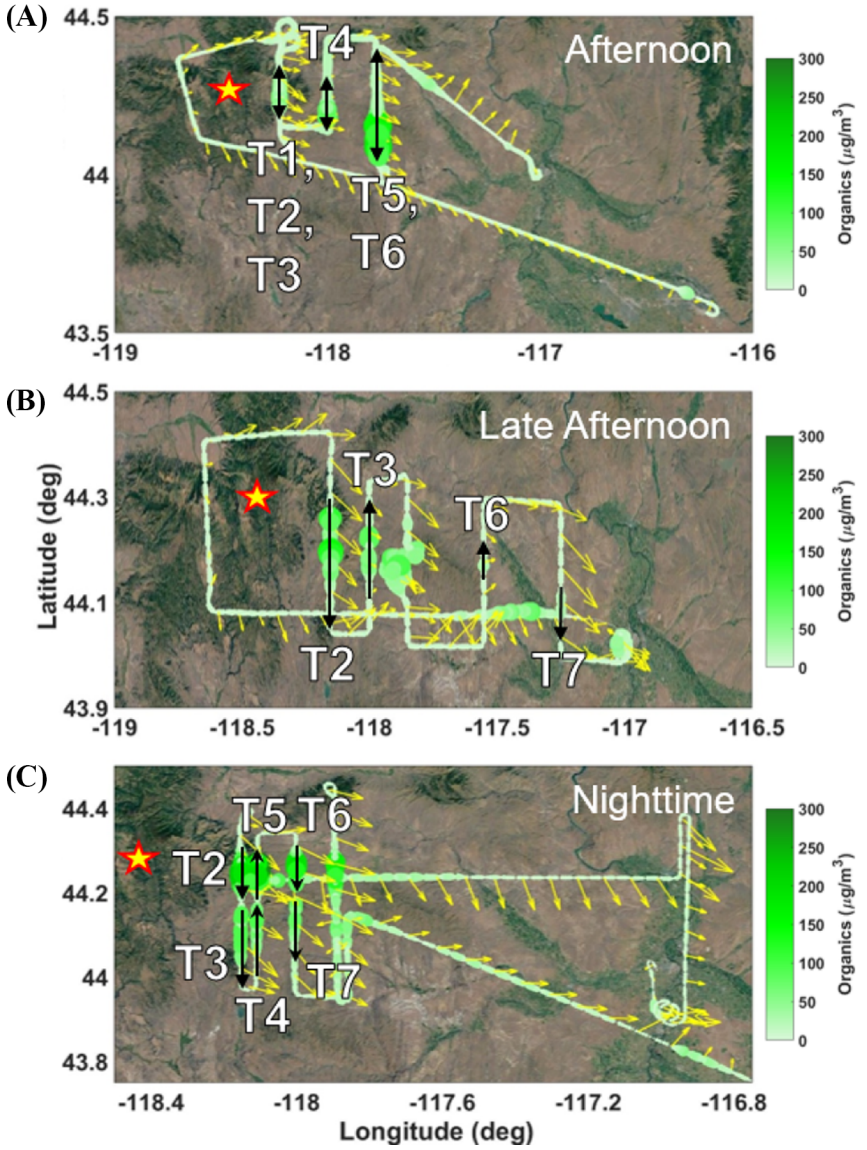

Flight	Plume Transect	Plume Age Average (hour) ± Uncertainty
L1/Afternoon	T3	0.66 ± 0.09
	T2	0.71 ± 0.09
	T1	0.78 ± 0.12
	T4	1.20 ± 0.10
	T6	1.61 ± 0.13
	T5	1.76 ± 0.15

Flight	Plume Transect	Plume Age Average (hour) ± Uncertainty
L2/Evening	T2	1.26 ± 0.28
	T3	1.67 ± 0.37
	T6	2.33 ± 0.55
	T7	2.89 ± 0.37

Flight	Plume Transect	Plume Age Average (hour) ± Uncertainty
L3/Nighttime	T2	2.19 ± 0.34
	T5	2.35 ± 0.29
	T6	2.47 ± 0.22
	T3	2.61 ± 0.39
	T4	2.71 ± 0.34
	T7	2.96 ± 0.27

Figure 1. Maps of flight trajectories within August 28, 2019 (A) afternoon, (B) late afternoon, and (C) night flights. The data points are color- and size-scaled to show AMS-derived organic mass concentration ($\mu g\ m^{-3}$) downwind of the emission source (marked with red and yellow star). Black lines and labels mark smoke plume transects and follow the trajectory of the flight path. Orientation and length of yellow arrows are qualitative representations of wind directions and speeds, respectively. Tables list averaged plume age time and its uncertainty corresponding to the individual transects in each flight. Transects are sorted based on the increasing plume age averages. Time periods of three flights are 12:44−15:22 (afternoon), 16:24−18:37 (late afternoon), and 19:32−22:07 (nighttime) reported as local time (PDT). Transects sampled at different altitudes have been disregarded in this study.

events, depending on biofuel type and moisture, burning phase (e.g., flaming versus smoldering), time of day, and other variables.[16−22]

A combination of multiphase chemical reactions and gas-particle partitioning processes transform BBA particles during the transport downwind of the emission zone.[14] In addition to processes of plume dilution, the size distribution and mass loadings of BBA change due to coagulation and gas-particle condensation of secondary products.[23−25] The rate of particle growth in biomass burning smoke plumes is strongly affected by environmental factors, including intensity of the sunlight, particle size, number concentration, ambient temperature and pressure.[26−29] Smoke plume transport also induces chemical and morphological transformations of the primary emitted BBA particles. A common observation is the substantial increase of secondary organic species in aged smoke particles resulting from the condensation of low volatility organic and inorganic components, such as oxygenated organics, nitrates, sulfates, and ammonium.[25,28,30−35] Furthermore, the water content of particles may increase when BBA organic material is internally mixed with hygroscopic inorganic salts. This can alter their reactivity, light-absorption, and propensity to act as cloud condensation nuclei (CCN).[36,37] The considerable variability in composition and particle characteristics poses significant challenges for atmospheric models in accurately representing the weather, climate, and health impacts of smoke. Consequently, additional field studies are needed to improve forecasts of the local and regional impacts of biomass burning emissions on the atmospheric environment and climate forcing.

We present measurements collected onboard the NOAA Twin Otter research aircraft during the 2019 Fire Influence on

https://doi.org/10.1021/acsearthspacechem.4c00215
ACS Earth Space Chem. XXXX, XXX, XXX−XXX

Regional to Global Environments and Air Quality (FIREX-AQ) field study.[38] This field campaign aimed at improving the understanding of wildfire and agricultural fire impacts on air quality, weather, and climate across the continental United States.[39,40] Here, we focus on data from three flights on August 28, 2019 which sampled smoke from the 204 Cow fire (point of initial wildfire 44.29°N, 118.46°W) during the afternoon, late afternoon, and at night.[18,38,41] We discuss a range of real-time airborne measurements of condensed- and gas-phase species normalized against carbon monoxide (CO) mixing ratios, featuring a comprehensive assessment of chemical composition and dilution-driven transformations of BBA downwind of the fire zone. We evaluate fire intensity metrics and total actinic fluxes derived for individual plume transects across the three flights, providing insight on key factors governing the initial chemical composition and reactivity of BBA from a midsize wildfire during atmospheric aging.

EXPERIMENTAL SECTION

Overview of the Field Campaign and Plume Age Calculations. The FIREX-AQ field study included 39 science flights by the NOAA "Chemistry" Twin Otter aircraft during August 3 to September 5, 2019. In this study, we focus on measurements acquired during August 28 as this was the only day with three distinct flights with high-quality data corresponding to plume transects sampling the same emission source, the 204 Cow fire.[41] To facilitate comprehensive chemical analysis of the smoke plume during atmospheric aging, flight transects began in close proximity to the emission source and then systematically traversed the aged plumes at progressive distances downwind of the fire. Such pattern, combined with the Twin Otter aircraft flight speed (65−75 m s^{-1}), resulted in data acquisition and sampling of BBA particles along near-Lagrangian flight trajectories.[41] Consequently, plume crossings performed within a particular flight are assumed to sample BBA particles emitted at the same time period.

The 204 Cow fire was started by lightning on August 9, 2019 and burned a total of 14.24 km^2 (shown in mission archives)[42] of mainly forest during August 28 when the aircraft sampling was conducted. Metrics on burned area were derived from NASA's Visible Infrared Imaging Radiometer Suite (VIIRS) satellite. The fire burned in the mountains of the Malheur National Forest in eastern Oregon, U.S. The GOES-16 fire radiative power (FRP) for this fire varied drastically over the course of this day, resulting in changes in fire emissions with time.[41] Figure 1 shows the flight tracks of the three flight legs (L1, L2, and L3) during afternoon (12:44−15:22 PDT), late afternoon (16:24−18:37 PDT), and nighttime (19:32−22:07 PDT), respectively. For each flight, a minimum of four plume transects were sampled, which provides an extensive assessment of the changes in BBA composition with respect to the fire's plume age over the course of a single day. The sun set at approximately 18:39 PDT on this date. Individual transects were manually defined based on CO measurements, serving as temporal markers for a structured analysis of evolving composition and physical properties of BBA. Specifically, instances of CO concentrations exceeding the background (150 ppb) are indicative of smoke plume transects. To distinguish between overlapping transects, 3D representations of flight trajectories are presented in Figure S1. A description of smoke plume age derivation is included in Supplementary Note 1. Briefly, this metric was estimated using multiple high-resolution meteorological data sets, including High-Resolution Rapid Refresh (HRRR), North American Mesoscale Forecast System (NAM) CONUS Nest, and Global Forecast System (GFS 0.25°), and by assuming a vertical plume rise of 7 m s^{-1}.[41] Plume age corresponding to the individual transects are listed in Figure 1 along with their uncertainties.

Online Measurements Onboard Research Aircraft. CO levels were measured with near-infrared cavity ring-down spectroscopy (G2401-m, Picarro Inc., Santa Clara, CA, USA).[43,44] Aerosol composition was measured with a high-resolution time-of-flight aerosol mass spectrometer instrument (HR-ToF-AMS, Aerodyne Research Inc., Billerica, MA, USA).[45,46] The AMS instrument measures concentrations of nonrefractory condensed-phase chemical species (μg std m^{-3} of air), including organic compounds, NH_4^+, SO_4^{2-}, NO_3^-, and Cl^-. The contribution of organo-sulfur compounds to the measured aerosol sulfate could not be determined for this data set.[47] The AMS was also used to derive the average oxidation states of carbon ($\overline{OS}_C$) and oxygen-to-carbon (O/C) ratio metrics,[48,49] as well as the mass concentrations of nitrocatechol for each transect.[41] Concentrations of gas-phase chlorinated species and nitric acid were determined using an iodide-adduct high-resolution time-of-flight chemical-ionization mass spectrometer (I^- CIMS).[50,51]

Real-time light absorption measurements were acquired using a particle-into-liquid sampler coupled to a liquid wavelength capillary cell and total organic carbon analyzer (BrC-PILS), described elsewhere.[41,52] Absorption at 400 nm wavelength (Abs_{400nm}) was subsequently used to calculate the water-soluble organic carbon mass absorption coefficient (MAC_{400nm}) attributed to the light absorbing organics, commonly referred to as "brown carbon" (BrC), as per the following equation:[41]

$$\text{BrC MAC}_{400\text{nm}} = \frac{\text{Abs}_{400\text{nm}}}{[\text{WSOC}]} \quad (1)$$

where [WSOC] is the mass concentration of water-soluble organic carbon, also measured by the BrC-PILS instrument. Light absorption was further evaluated within the 310−440 nm wavelength range to determine the absorption Ångström exponent (AAE), which relates to light absorption coefficients (C_{abs}) and wavelengths (λ) as per the following equation:[53]

$$\text{AAE} = \frac{\ln(C_{abs1}/C_{abs2})}{\ln(\lambda_1/\lambda_2)} \quad (2)$$

RESULTS AND DISCUSSION

BBA particles contain three general components: organic material, black carbon (soot), and inorganic species. The mass concentrations and mixing ratios of these components within discrete smoke plumes depend strongly on the nature of burned biomass, as well as environmental and burning conditions, thereby yielding multicomponent BBA emissions. Figure 2 shows the absolute mass concentrations of non-refractory, condensed-phase organic material and inorganic species, measured by an HR-ToF-AMS instrument across afternoon, late afternoon, and nighttime plumes. The initial mass concentrations of both organic and inorganic constituents show substantial differences between three plumes, with lower concentrations observed in the afternoon and late afternoon plumes compared to the nighttime plume. These discrepancies reflect diurnal variations in fire intensity represented as FRP,

https://doi.org/10.1021/acsearthspacechem.4c00215
ACS Earth Space Chem. XXXX, XXX, XXX−XXX

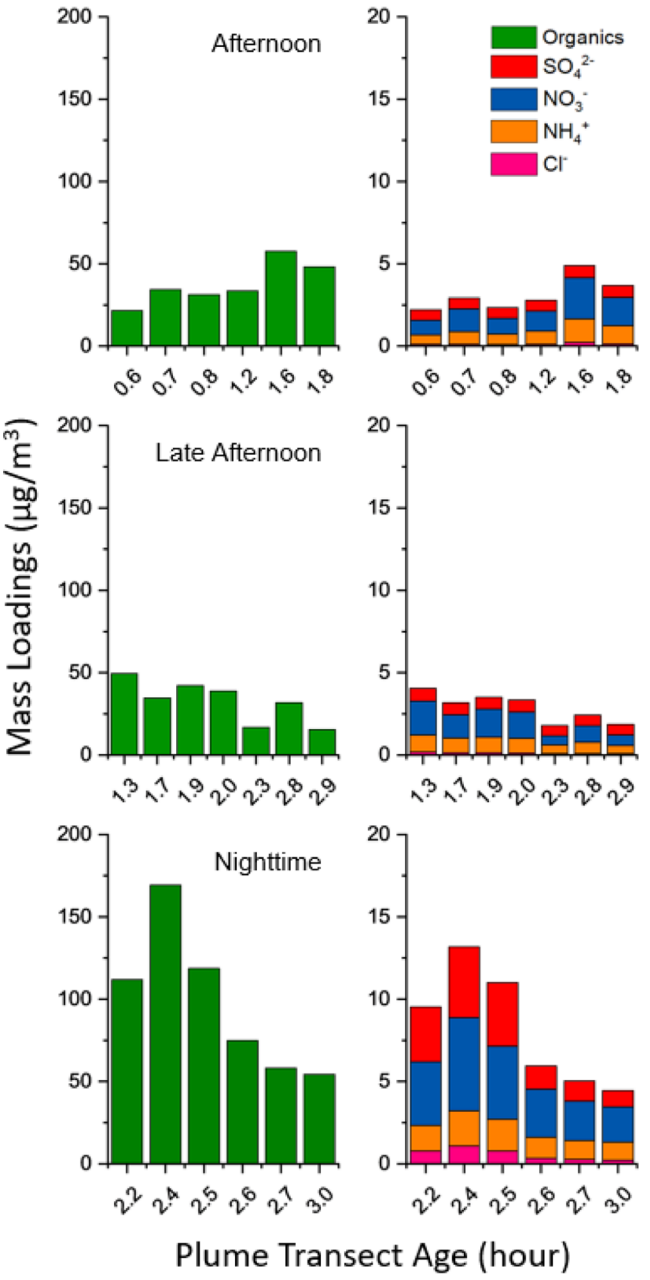

Figure 2. Airborne absolute mass loadings of BBA components measured within afternoon (top), late afternoon (middle), and nighttime (bottom) plumes. The mass loadings of organic components are consistently about ten times higher than the combined mass loadings of inorganic components.

which was derived from GOES-16 data for each plume transect at the time of emission and average combustion conditions, as illustrated in Figure S2. For BBA measured in the afternoon and night flights, FRP remained below 500 MW, while fire intensity corresponding to the late afternoon plume was above 800 MW. Additionally, FRP showed an inverse correlation with the mass concentrations of organic aerosols, with the nighttime flight presenting the lowest FRP values (<250 MW) and highest concentration of organics with respect to CO. To evaluate the impact of burning conditions on the concentration of organic material, FRP was also correlated with the modified combustion efficiency (MCE), a metric used to differentiate between smoldering and flaming burning conditions. MCE was calculated for individual plume transects as described in Supplementary Note 2. Figure S2 shows that both metrics are positively correlated, with lower MCE associated with smaller FRP and enhanced mass concentrations of organic BBA. This observation aligns with a previous study,[16] which showed that the emission of organic material in biomass burning events is substantially increased when the fire is characterized by low MCE values, corresponding to smoldering burning conditions. Despite the differences in the absolute mass concentrations between three flights, the organic components constitute ~89−93% of the AMS-derived total particle mass, with the remaining ~7−11% ascribed to combined contributions from sulfate (SO_4^{2-}), nitrate (NO_3^-), nonrefractory chloride (Cl^-), and ammonium (NH_4^+) (see Figure S3). Measurements reported in Figure 2 further indicate that atmospheric processes such as dilution and aging chemistry induce alterations in the particle mass concentrations along the plume transported downwind of the fire zone. Inorganic aerosol mass loadings increase with plume age during afternoon, which is likely due to the contributions of photochemical oxidation and subsequent formation of low volatility secondary products. Conversely, inorganic aerosol mass loadings decline along the plumes probed in the late afternoon and the nighttime flights.

Decreases in absolute aerosol mass concentrations with age could indicate dilution and mixing. Given the substantial emissions of CO during biomass burning events and its slow atmospheric reactivity, online measurements collected within individual transects were compared and scaled against concentrations of this gas as a quantitative metric to account for plume dilution and discern plume evolution.[54] Figure 3 displays mass concentrations of organic aerosol, measured by AMS and normalized to CO mixing ratios, presented for each of the three flights as a function of the transect age time. The afternoon plume exhibits increasing dilution-corrected organic aerosol mass as a function of plume age. In contrast, the late afternoon and nighttime plumes lose organic aerosol mass as a function of plume age. The potential processes responsible for these differences are evaporation of the condensed-phase organic material (mass loss) and photochemical production of secondary aerosol species (mass gain), or a combination of the two resulting in a net of either mass gain or mass loss. Composition of the organic components in both the gas and aerosol phase, photochemical conditions (or lack thereof), temperature, relative humidity, and dilution rate can play various roles in these processes.[33] Plume crossings during the afternoon flight show an increase of particle-phase organics downwind of the emission source. The observed buildup aligns well with previously reported transformations in the biomass burning plume attributed to photochemical oxidation of the gas-phase emissions and subsequent condensation of their oxidized low vapor pressure products onto existing particles.[14,55,56] Furthermore, concentrations of ozone peak during the afternoon flight (Figure S4), suggesting that additional oxidation processes are potentially occurring during this day period. Photochemical oxidation during the late afternoon flight is significantly reduced and formation of secondary organic material is limited, resulting in an overall depletion of organics with respect to plume age. Moreover, the aerosol sampled at night was likely emitted in the last hour before sunset, with weak sunlight available and a short amount of time for photochemical reactions before sampling. Nighttime reactions involving NO_3 or O_3 oxidation may lead to secondary

https://doi.org/10.1021/acsearthspacechem.4c00215
ACS Earth Space Chem. XXXX, XXX, XXX−XXX

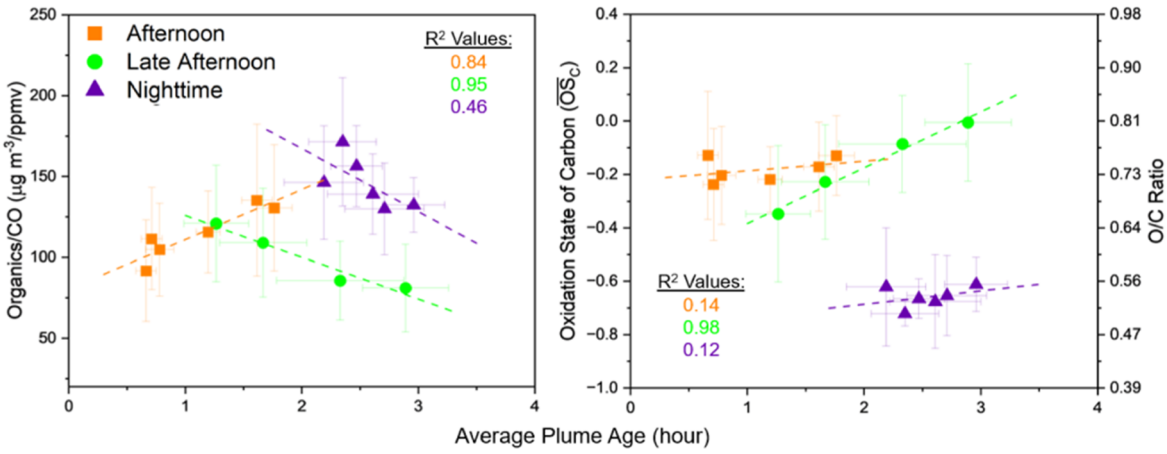

Figure 3. Evolution of condensed-phase organic mass loadings (left panel) and AMS-derived oxidation state of carbon ($\overline{OS}_C$) and oxygen-to-carbon (O/C) ratios (right panel) in afternoon, late afternoon, and night plumes. Error bars represent the standard deviation of the measurement averages representative of individual plume transects. Dashed lines correspond to the linear fits of the data sets. R^2 values for fit lines are included for a qualitative examination of the correlation between both data sets.

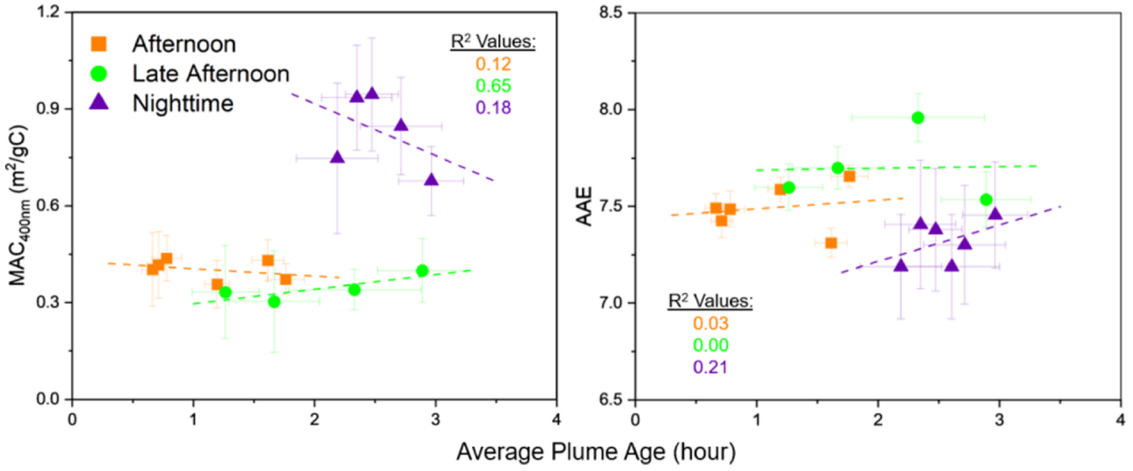

Figure 4. Evolution of water-soluble organic carbon mass absorption coefficient at 400 nm (MAC_{400nm}) and absorption Ångström exponent (AAE) in afternoon, late afternoon, and night plumes. Error bars represent the standard deviation of the measurement averages representative of individual plume transects. Dashed lines correspond to the linear fits of the data sets. R^2 values for fit lines are included for a qualitative examination of the correlation between both data sets.

organic aerosol (SOA) production,[18,57] but if so, this SOA production is slower than OA loss in this case. Discrepancies in the photochemical activity between three flights were quantified with the Tropospheric Ultraviolet and Visible radiation model, as depicted in Figure S5. In agreement with previous study,[58] the total actinic flux is higher during the afternoon flight and progressively decreases, reaching zero at night. The net effect of inhibited photochemical reactions together with dilution-driven evaporation during the late afternoon and nighttime flights is that their organic mass loadings decreased with age.[59]

Figure 3 also shows the average $\overline{OS}_C$ and O/C ratios calculated from AMS records for individual transects across the three flights. The average $\overline{OS}_C$ values in BBA for the nighttime plume are significantly lower compared to the daytime plumes. Changes in the $\overline{OS}_C$ and O/C ratio for BBA with plume age reflect a combination of dilution-driven evaporation which can result in loss of less oxidized species and photochemistry that causes condensation of more oxidized species.[33] BBA oxidation during afternoon and late afternoon is further enhanced by NO_3 oxidation reactions, which are active during daytime due to the increased production of nitrates and high reactivity of volatile organic compounds (VOCs).[18] For the three types of plumes sampled, only the late afternoon plume showed a significant increase in $\overline{OS}_C$ and O/C ratios with respect to plume age which is indicative of the higher degree of these oxidation processes at that time of day compared to the other times.

Without knowing the exact history of the plumes between the time of emission and subsequent sampling, we can only hypothesize on the reasons for the observed net effects on the plume aging properties. Satellite FRP data indicates that the fire intensity varied significantly throughout the day when the plumes were emitted, affecting the composition of both the BBA and the VOCs at the time of emission. Consequently, the organic species that evaporate or condense while aging vary at different times of the day. As the organic aerosol mass ratio to CO increased for the afternoon plume while the $\overline{OS}_C$ and O/C ratios remained relatively constant, the balance of organic species involved in these processes did not significantly alter

https://doi.org/10.1021/acsearthspacechem.4c00215
ACS Earth Space Chem. XXXX, XXX, XXX−XXX

the overall average organic aerosol composition. The smaller organic mass loss observed in the plume sampled at night, with only a slight increase in average $\overline{OS}_C$ and O/C ratios, suggests that the less oxidized species were less affected by sunlight-induced and NO_3 oxidation reactions, and by less evaporation due to cooler temperatures after sunset (see Figure S6). In contrast, the late afternoon plume showed the clearest signals of net evaporation with an expected increase in oxidation.

Evaporation of particle components in BBA plumes upon dilution has been correlated to the evolution of BrC optical properties, predominantly reporting on the darkening of BBA particles in previous studies.[60−62] Figure 4 shows the water-soluble organic carbon MAC_{400nm} and AAE derived from in situ PILS-BrC measurements averaged over each plume transect from all three flights. Despite the different trends in organics/CO ratios with plume age (Figure 3), these optical metrics illustrate only slight differences in the BrC light absorption as a function of plume age throughout each of the three flights, indicating no substantial BrC darkening or bleaching in the aged plumes at the time range of our flights. The relative optical stability of BrC in these plumes was also reported based on the $MAC_{365\ nm}$ values published earlier.[41] However, it is important to note that the light absorption measured by the PILS-BrC instrument is determined from the concentration of water-soluble organic compounds as defined by eq 1. Hence, variability in the solubility of light-absorbing species, induced by aging and photochemistry, will result in change of MAC and AAE values. While light absorption by BrC does not evolve significantly within the sampled plumes, discernible differences are observed between each of the three plumes. Specifically, the nighttime BrC MAC_{400nm} values are twice as large as those measured in the afternoon and late afternoon plumes. These observed differences likely reflect variations in initial burning conditions and FRP, concurrently leading to variability in the content of common BrC chromophores, such as nitrophenols.[63] As shown in Supplementary Note 5, nighttime BBA particles exhibited enhanced AMS-derived mass concentrations of nitrocatechol, a prominent atmospheric nitrophenol formed from NO_x reactions with biomass burning emissions.[63−65] While nitrocatechol may not be the dominant chromophore present, it contributed a slightly larger fraction of the total particle mass at night compared to afternoon and late afternoon samples, and showed a positive correlation with MAC_{400nm} (see Figure S8). This suggests that other similar species may also contribute to the optical properties of strongly absorbing BBA. Given that all three flights sampled smoke particles emitted from the same fire event, variations in biomass fuel type are a less likely explanation for the observed variability in MAC at different times of the day. The most likely reason for the differences is that the plumes sampled at night were emitted when the fire intensity was low before sunset.

While the organic mass fraction of the BBA measured by the AMS was above 89%, the inorganic fraction was not insignificant (see Figure S3). The high hygroscopicity of the inorganic material defines the water-uptake characteristics of BBA particles when internally mixed with organic material.[36,37] Consequently, it is crucial to examine noncarbonaceous species emitted from fire events, as the humidification of BBA through inorganic-induced hygroscopic growth impacts its chemical reactivity, optical properties, and propensity to act as CCN.[66,67] The composition of inorganic components was systematically assessed based on the molar ratios of the most common NH_4^+, SO_4^{2-}, NO_3^-, and Cl^- inorganic species. Figure 5 shows the average cation-to-anion ratios derived from

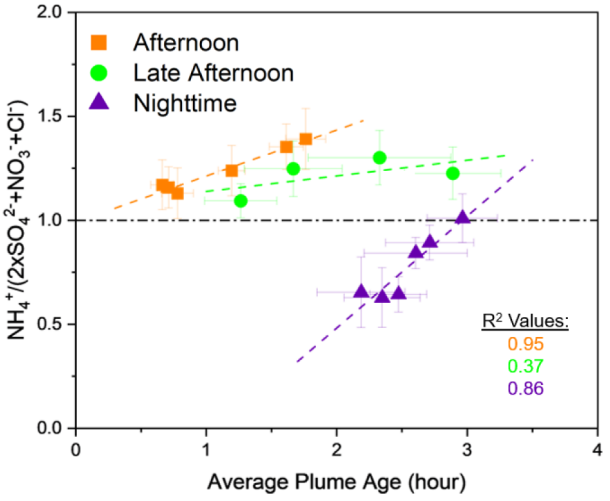

Figure 5. Average AMS-derived cation-to-anion ratios corresponding to afternoon, late afternoon, and nighttime plume transects. The ratio is determined from the ions molar masses and defined as $(NH_4^+/18)/(2\times SO_4^{2-}/96 + NO_3^-/62 + Cl^-/35.5)$. The black dashed line represents a cation-to-anion ratio = 1. Error bars represent the standard deviation of the measurement averages representative of individual plume transects. Dashed lines correspond to the linear fits of the data sets. R^2 values for fit lines are included for a qualitative examination of the correlation between both data sets.

AMS measurements during three different flights. A molar balance ratio of $NH_4^+/(2\times SO_4^{2-} + NO_3^- + Cl^-)$ equal to 1 indicates complete neutralization of SO_4^{2-}, NO_3^-, and Cl^- through the formation of $(NH_4)_2SO_4$, NH_4NO_3, and NH_4Cl salts.[68] The ratios of 1.0−1.5 observed for the afternoon and late afternoon flights indicate complete neutralization of common inorganic acids in BBA along with contributions of additional ammonium salts, likely related to neutralization of organic carboxylic acids, which has been previously reported for daytime biomass burning events.[69] Conversely, lower ratios of 0.5−1.0 common in the nighttime plume indicate acidity of BBA, especially in younger plume transects. The acidity of BBA was inferred from the Extended Aerosol Inorganics Model (E-AIM) (https://www.aim.env.uea.ac.uk/aim/aim.php).[70] The pH values of particles sampled across the three flights ranged between 2 and 3, in agreement with values reported for air masses impacted by biomass burning events.[71] It is important to note that if a fraction of the reported AMS nitrate and sulfate mass is due to organo-sulfates and organo-nitrates, the actual ratios would be higher. Moreover, AMS is less sensitive to KCl due to its refractory nature at the temperature used to vaporize incoming aerosols (~600 °C).[45] Given that KCl is a major source of condensed-phase chlorine emitted during biomass burning, AMS measurements underestimate Cl^- mass concentrations.

Figure 6 illustrates the temporal evolution of individual condensed-phase NH_4^+, SO_4^{2-}, NO_3^-, and Cl^- components. Afternoon measurements show a simultaneous buildup of NH_4^+ and NO_3^-, associated with photochemically driven gas-phase formation of nitric acid as well as organic nitrates from NO_x, followed by partitioning into particle phase with nitric acid and ammonia combining to produce ammonium nitrate.[72,73] Different from the afternoon and nighttime, a

https://doi.org/10.1021/acsearthspacechem.4c00215
ACS Earth Space Chem. XXXX, XXX, XXX−XXX

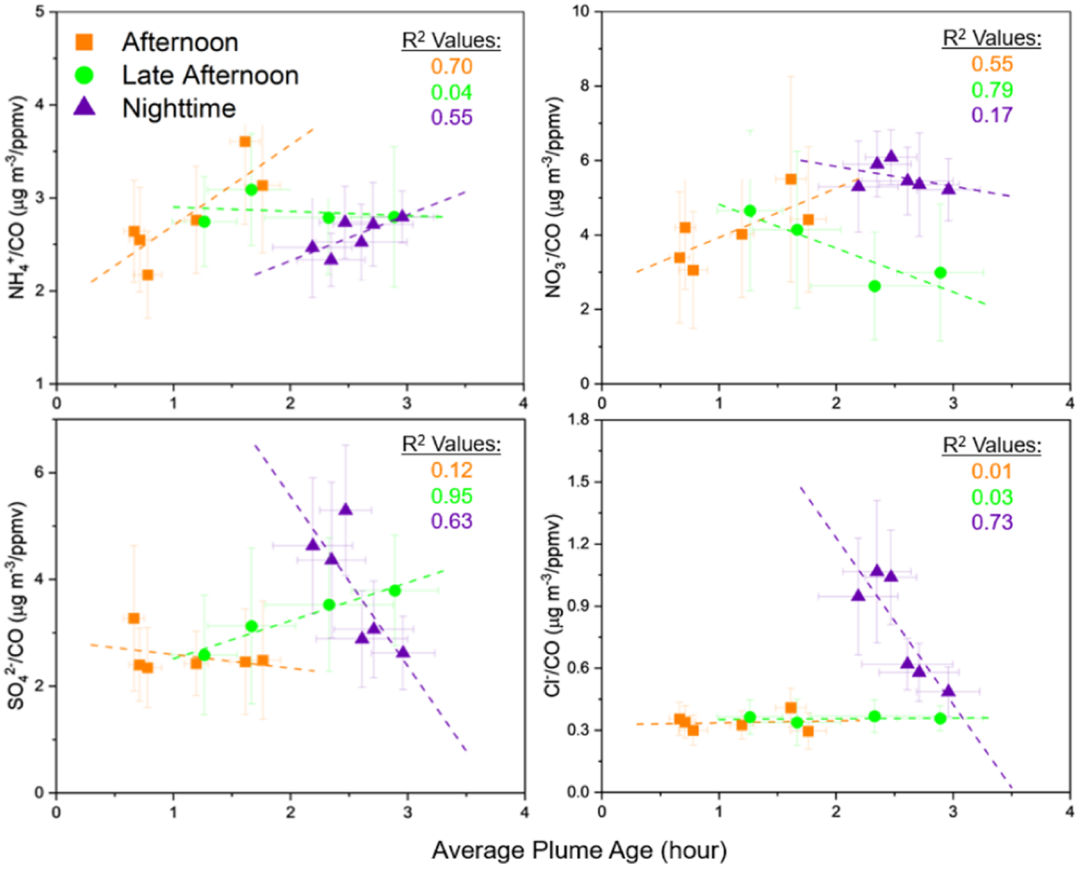

Figure 6. Evolution of condensed-phase NH_4^+, NO_3^-, SO_4^{2-}, and Cl^- mass loadings within afternoon, late afternoon, and nighttime plumes. Error bars represent the standard deviation of the measurement averages representative of individual plume transects. Dashed lines correspond to the linear fits of the data sets. R^2 values for fit lines are included for a qualitative examination of the correlation between both data sets.

noticeable decay of NO_3^- mass loadings with respect to CO is observed upon aging of the late afternoon plume, likely reflecting evaporation of NH_4NO_3 back to its gas-phase components of NH_3 and HNO_3 driven by plume dilution, as per the following chemical reaction:

$$NH_4NO_{3(particle)} \leftrightarrow NH_{3(g)} + HNO_{3(g)} \quad (R1)$$

The evolution of condensed-phase NO_3^- with respect to plume age, measured during the afternoon and late afternoon flights, aligns with the predicted gas-particle partitioning of HNO_3 and NO_3^- derived from the E-AIM model, as shown in Figure S9. HNO_3/NO_3^- decreases as the plume ages during the afternoon, due to formation of NH_4NO_3; whereas the partitioning during late afternoon favors the degassing and subsequent buildup of HNO_3 in the gas-phase. Differently, no overlap is observed between HNO_3/NO_3 ratios measured during the nighttime and those calculated by the E-AIM model, which underestimates the contribution of particle-phase NO_3^-. This discrepancy is likely a result of unaccounted common cations such as K^+ and Ca^{2+}, which form nitrate salts that are not included in the model. This aligns with findings from our previous single-particle study,[74] where levels of potassium-containing species were reported to be higher during the nighttime. Moreover, the equilibrium of reaction R1 is an interplay between the photochemical formation of nitric acid, relative humidity (RH), ambient temperature, and dilution effects in the evolving plumes. As a result, changes in the mass loadings of the condensed phase NO_3^- are mirrored by changes in the mixing ratios of the gas-phase HNO_3, as illustrated in Figure S10. The inverse quantitative relationship between NO_3^- and HNO_3 concentrations is notably distinct in the daytime plumes, highlighting the significance of this equilibrium in the biomass burning plumes. The nighttime trend differs, with NO_3^- concentrations consistently higher than those of gas-phase HNO_3, and no reciprocal changes observed. This nighttime pattern could be due to stabilization of the aerosol nitrate when the air mass cools after sunset as well as higher RH (see Supplementary Note 4 for meteorological measurements), which favors NH_4NO_3 to remain in the condensed phase. Despite of the trends in the evolution of NO_3^- being primarily attributed to environmental factors, discrepancies between nitrate concentrations across the three flights may be dictated by variability in burning conditions at the emission source. Mass loadings of SO_4^{2-} measured in the same plume during the afternoon remain nearly constant, indicating that levels of particulate sulfates are largely governed by the emission source.[47] A gradual increase of SO_4^{2-} is observed in the late afternoon plume with respect to plume age, whereas the dilution-corrected SO_4^{2-} decreases in the nighttime plume. These trends in condensed-phase SO_4^{2-} are consistent with findings from a previous biomass burning study.[75] Specifically, sunlight exposure during the daytime enhances the production of oxidative species, including H_2O_2 in the atmospheric water, driving the buildup of SO_4^{2-} through aqueous-phase oxidation of SO_2.[76] This aligns with the $\overline{OS}_C$ and O/C ratios reported in Figure 3, which indicates more extensive aerosol oxidation in the late afternoon plume compared to the nighttime. Formation of

https://doi.org/10.1021/acsearthspacechem.4c00215
ACS Earth Space Chem. XXXX, XXX, XXX−XXX

sulfates downwind of the fire zone during late afternoon is further supported by the increasing mass fraction of SO_4^{2-} shown in Figure S3. In contrast, the decay of SO_4^{2-} during the nighttime may reflect the loss of short-lived organo-sulfur species formed through the reaction of oxygenated organics with sulfuric acid generated by oxidation of SO_2.[35,47] Additionally, the discrepancies in the evolution of SO_4^{2-} between afternoon and late afternoon flights may be attributed to differences in the burning conditions at the emission source, despite both sampling periods experiencing comparable sunlight exposures (Figure S5).

Figure 6 also shows mass loadings of condensed-phase Cl^- observed in three plumes. Compared to other inorganic components, contributions of Cl^- are minor, accounting for only a small percentage of the total AMS components (see Figure S3). Chlorine in fire events primarily originates from particles containing KCl salts emitted by the burning of specific types of biomass.[14] In the afternoon and late afternoon plumes, nonrefractory chloride measured by the AMS remained relatively constant with respect to CO. However, in the nighttime plume, Cl^- was relatively enhanced closer to the fire zone but showed significant depletion in aged BBA particles. Similar trends are observed when comparing the mass fraction of Cl^- across the three flights. Due to the limited sensitivity of AMS toward KCl, the observed loss of nonrefractory chloride from aerosol is attributed to the degassing of highly volatile HCl following the gas-particle partitioning of NH_4Cl, which forms via reversible equilibrium with precursor gases NH_3 and HCl.[77]

$$NH_4Cl_{(aq)} \leftrightarrow NH_{3(aq,g)} + HCl_{(aq,g)} \quad (R2)$$

NH_4Cl is more thermodynamically stable in fully neutralized particles, such as those observed in the afternoon and late afternoon plumes. However, NH_3 and HCl can evaporate from the hygroscopically grown BBA particles with higher water content in the nighttime plume, which exhibit higher acidity (see Figure 5). Furthermore, chloride in nighttime BBA particles with higher water content may react with organic acids, releasing HCl gas into the atmosphere and leaving chloride-depleted particles enriched in organic salts.[78] Regardless of the time of day, the molar concentration of gaseous HCl measured in the plumes are ~10 times larger than the available condensed-phase Cl^-, as illustrated in Figure S11. This difference likely suggests that large amounts of HCl are formed from chlorine in the form of primarily emitted KCl, which is less efficiently measured by the AMS due to its thermodynamic stability. Consequently, concentrations derived from AMS underestimate the real contribution of chlorine-containing species to the total particle mass. Discrepancies between HCl and Cl^- can also be influenced by the relatively higher vapor pressure of gas-phase HCl compared to gas-phase HNO_3 for systems containing both NH_4NO_3 and NH_4Cl,[70] enhancing the concentration of HCl in the ambient. Concentrations of the condensed-phase Cl^- are on par with the observed gas-phase concentrations of nitryl chloride ($ClNO_2$), which is likely formed through the particle-phase hydrolysis of N_2O_5, followed by the reaction with dissolved Cl^- and the evaporation of $ClNO_2$, summarized below.[79,80]

$$N_2O_{5(aq)} + H_2O_{(aq)} \leftrightarrow H_2O{\cdot}NO_{2(aq)}^+ + NO_{3(aq)}^- \quad (R3)$$

$$H_2O{\cdot}NO_{2(aq)}^+ + Cl_{(aq)}^- \rightarrow ClNO_{2(aq,g)} \uparrow + H_2O_{(aq)} \quad (R4)$$

Photolysis of the $ClNO_{2(g)}$ products will therefore increase atmospheric radical oxidants.

CONCLUSIONS

In this study, we assessed particle- and gas-phase constituents and optical properties of aerosols within the biomass burning plumes originating from the 204 Cow fire, a midsized wildfire, during the FIREX-AQ field study. These measurements were conducted over a single day in a near-Lagrangian manner to evaluate how the chemical composition and optical properties vary at different times of the day. Real-time aerosol mass spectrometry measurements were examined to provide insights into the dynamic evolution of nonrefractory aerosol components. The presented data underscores complex interplay of environmental factors and emission sources on BBA composition, offering insights into the dynamic nature of aerosol particle transformations and behavior during different time periods for the same wildfire. The chemical composition differed depending on the time of day when the BBA was emitted and sampled, and was plausibly influenced by the burning conditions at the fire zone. Compared to the afternoon and late afternoon BBA, the nighttime aerosol composition was generally less oxidized, contained insufficient ammonium to balance the measured anions, and presented relatively more nitrate, nitrocatechol and nonrefractory chloride. Photochemically driven increases in the concentrations of condensed-phase organics, NH_4^+, and NO_3^- were observed in the afternoon as a function of plume age. In contrast, a discernible depletion of organic and nitrate components occurred in the late afternoon. While nonrefractory chloride was relatively higher in the nighttime plume, it decreased to levels similar to those observed in the afternoon and late afternoon. Despite variations in the evolution trends of chemical species across three plumes, the optical metrics of BrC components (MAC_{400nm} and AAE) showed no major changes with atmospheric aging. Light absorption by BrC was different between each of the plumes, where nitrocatechol was indicative of more absorption at night. Overall, this study of a single wildfire plume over 1 day demonstrates that the BBA composition, optical properties, and subsequent attributes due atmospheric aging are variable. This suggests that differences in emissions at the source, the amount of sunlight available for photochemistry, and daytime versus nighttime NO_3 chemistry were crucial for understanding how BBA evolve in the initial few hours after emission.

ASSOCIATED CONTENT

Supporting Information

The Supporting Information is available free of charge at https://pubs.acs.org/doi/10.1021/acsearthspacechem.4c00215.

3D flight maps; plume age calculations; FRP and MCE calculations; mass fractions; meteorological measurements; TUV model; nitrocatechol concentrations; E-AIM model (PDF)

AUTHOR INFORMATION

Corresponding Author

Alexander Laskin − *Department of Chemistry, Purdue University, West Lafayette, Indiana 47907, United States; Department of Earth, Atmospheric and Planetary Sciences, Atmospheric and Planetary Sciences, Purdue University, West*

https://doi.org/10.1021/acsearthspacechem.4c00215
ACS Earth Space Chem. XXXX, XXX, XXX−XXX

Lafayette, IN 47907, USA; orcid.org/0000-0002-7836-8417; Email: alaskin@purdue.edu

Authors

Felipe A. Rivera-Adorno − *Department of Chemistry, Purdue University, West Lafayette, Indiana 47907, United States;* orcid.org/0000-0002-7355-7999

Lisa Azzarello − *Department of Chemistry, York University, Toronto, ON M3J 1P3, Canada;* orcid.org/0000-0002-5348-1595

Michael A. Robinson − *Chemical Sciences Laboratory, National Oceanic and Atmospheric Administration, Boulder, CO 80305, USA; Cooperative Institute for Research in Environmental Sciences, University of Colorado, Boulder, CO 80309, USA*

Zachary C. J. Decker − *Chemical Sciences Laboratory, National Oceanic and Atmospheric Administration, Boulder, CO 80305, USA; Cooperative Institute for Research in Environmental Sciences, University of Colorado, Boulder, CO 80309, USA;* orcid.org/0000-0001-9604-8671

Rebecca A. Washenfelder − *Chemical Sciences Laboratory, National Oceanic and Atmospheric Administration, Boulder, CO 80305, USA;* orcid.org/0000-0002-8106-3702

Katherine Hayden − *Air Quality Research Division, Environment and Climate Change Canada, Toronto, ON M3H 5T4, Canada*

Alessandro Franchin − *Atmospheric Chemistry Observations & Modelling Laboratory, University Corporation for Atmospheric Research, Boulder, CO 80307, USA*

Christopher D. Holmes − *Earth, Ocean, and Atmospheric Science, Florida State University, Tallahassee, FL 32306, USA;* orcid.org/0000-0002-2727-0954

Cora J. Young − *Department of Chemistry, York University, Toronto, ON M3J 1P3, Canada;* orcid.org/0000-0002-6908-5829

Carley D. Fredrickson − *Department of Atmospheric and Climate Science, University of Washington, Seattle, WA 98195, USA;* orcid.org/0000-0002-9127-5258

Brett Palm − *Department of Atmospheric and Climate Science, University of Washington, Seattle, WA 98195, USA;* orcid.org/0000-0001-5548-0812

Chris Schmidt − *Space Science and Engineering Center and Cooperative Institute for Meteorological Satellite Studies, University of Wisconsin, Madison, WI 53706, USA*

Amber Soja − *Climate Science, Chemistry and Dynamics Branches of Atmospheric Sciences, NASA Langley Research Center, Hampton, VA 23666, USA;* orcid.org/0000-0001-8637-3040

Emily Gargulinski − *Atmospheric Science Research Department, National Institute of Aerospace, Hampton, VA 23666, USA;* orcid.org/0000-0002-3949-6627

Steven S. Brown − *Chemical Sciences Laboratory, National Oceanic and Atmospheric Administration, Boulder, CO 80305, USA; Department of Chemistry, University of Colorado, Boulder, CO 80309, USA;* orcid.org/0000-0001-7477-9078

Ann M. Middlebrook − *Chemical Sciences Laboratory, National Oceanic and Atmospheric Administration, Boulder, CO 80305, USA;* orcid.org/0000-0002-2984-6304

Complete contact information is available at: https://pubs.acs.org/10.1021/acsearthspacechem.4c00215

Author Contributions

F.R. and A.L. devised the project. L.A., M.R., Z.D., R.W., K.H., A.F., C.H., C.Y., C.F., B.P., A.S., E.G., S.B., and A.M. worked on the acquisition and processing of online chemical and optical measurements. F.R., R.W., and A.M. analyzed and integrated all data sets. F.R. and A.L. wrote the manuscript with contributions from all coauthors.

Notes

The authors declare no competing financial interest.

■ ACKNOWLEDGMENTS

We acknowledge Colm Sweeney and Tim Newberger from the Global Monitoring Laboratory at NOAA for their stewardship of CO data. We thank Joel Thornton from the University of Washington for his supervision of CIMS data acquisition. The Purdue University group acknowledges partial support from discretionary startup funds allocated to A.L. and the U.S. Department of Energy's Atmospheric System Research Program, Office of Biological and Environmental Research (grant DE-SC0021977). C.D.F. and B.B.P. were supported by the NOAA OAR Climate Program Office (award number NA17OAR4310012). Z.D. was supported by a graduate research award from the Cooperative Institute for Research in Environmental Sciences. C.D.H. was supported by NASA (grant 80NSSC18K0625).

■ REFERENCES

(1) Andreae, M. O.; Merlet, P. Emission of Trace Gases and Aerosols from Biomass Burning. *Global Biogeochem. Cycles* **2001**, *15* (4), 955−966.

(2) Penner, J. E.; Dickinson, R. E.; O'Neill, C. A. Effects of Aerosol from Biomass Burning on the Global Radiation Budget. *Science* **1992**, *256* (5062), 1432−1434.

(3) Haywood, J.; Boucher, O. Estimates of the Direct and Indirect Radiative Forcing Due to Tropospheric Aerosols: A Review. *Rev. Geophys.* **2000**, *38* (4), 513−543.

(4) Pierce, J. R.; Chen, K.; Adams, P. J. Contribution of Primary Carbonaceous Aerosol to Cloud Condensation Nuclei: Processes and Uncertainties Evaluated with a Global Aerosol Microphysics Model. *Atmos. Chem. Phys.* **2007**, *7* (20), 5447−5466.

(5) Spracklen, D. V.; Carslaw, K. S.; Pöschl, U.; Rap, A.; Forster, P. M. Global Cloud Condensation Nuclei Influenced by Carbonaceous Combustion Aerosol. *Atmos. Chem. Phys.* **2011**, *11* (17), 9067−9087.

(6) Chen, J.; Li, C.; Ristovski, Z.; Milic, A.; Gu, Y.; Islam, M. S.; Wang, S.; Hao, J.; Zhang, H.; He, C.; et al. A Review of Biomass Burning: Emissions and Impacts on Air Quality, Health and Climate in China. *Sci. Total Environ.* **2017**, *579*, 1000−1034.

(7) de Oliveira Alves, N.; Brito, J.; Caumo, S.; Arana, A.; de Souza Hacon, S.; Artaxo, P.; Hillamo, R.; Teinilä, K.; Batistuzzo de Medeiros, S. R.; de Castro Vasconcellos, P. Biomass Burning in the Amazon Region: Aerosol Source Apportionment and Associated Health Risk Assessment. *Atmos. Environ.* **2015**, *120*, 277−285.

(8) Kaulfus, A. S.; Nair, U.; Jaffe, D.; Christopher, S. A.; Goodrick, S. Biomass Burning Smoke Climatology of the United States: Implications for Particulate Matter Air Quality. *Environ. Sci. Technol.* **2017**, *51* (20), 11731−11741.

(9) Lin, N.-H.; Tsay, S.-C.; Maring, H. B.; Yen, M.-C.; Sheu, G.-R.; Wang, S.-H.; Chi, K. H.; Chuang, M.-T.; Ou-Yang, C.-F.; Fu, J. S.; et al. An Overview of Regional Experiments on Biomass Burning Aerosols and Related Pollutants in Southeast Asia: From BASE-ASIA and the Dongsha Experiment to 7-SEAS. *Atmos. Environ.* **2013**, *78*, 1−19.

(10) McClure, C. D.; Jaffe, D. A. US Particulate Matter Air Quality Improves except in Wildfire-Prone Areas. *Proc. Natl. Acad. Sci. U.S.A.* **2018**, *115* (31), 7901−7906.

(11) Rappold, A. G.; Stone, S. L.; Cascio, W. E.; Neas, L. M.; Kilaru, V. J.; Carraway, M. S.; Szykman, J. J.; Ising, A.; Cleve, W. E.; Meredith, J. T.; et al. Peat Bog Wildfire Smoke Exposure in Rural North Carolina Is Associated with Cardiopulmonary Emergency Department Visits Assessed through Syndromic Surveillance. *Environ. Health Perspect.* **2011**, *119* (10), 1415−1420.
(12) Thelen, B.; French, N. H.; Koziol, B. W.; Billmire, M.; Owen, R. C.; Johnson, J.; Ginsberg, M.; Loboda, T.; Wu, S. Modeling Acute Respiratory Illness during the 2007 San Diego Wildland Fires Using a Coupled Emissions-Transport System and Generalized Additive Modeling. *Environ. Health* **2013**, *12* (1), 94.
(13) Yokelson, R. J.; Crounse, J. D.; DeCarlo, P. F.; Karl, T.; Urbanski, S.; Atlas, E.; Campos, T.; Shinozuka, Y.; Kapustin, V.; Clarke, A. D.; et al. Emissions from Biomass Burning in the Yucatan. *Atmos. Chem. Phys.* **2009**, *9*, 5785−5812.
(14) Reid, J. S.; Koppmann, R.; Eck, T. F.; Eleuterio, D. P. A Review of Biomass Burning Emissions Part II: Intensive Physical Properties of Biomass Burning Particles. *Atmos. Chem. Phys.* **2005**, *5*, 799−825.
(15) Li, J.; Pósfai, M.; Hobbs, P. V.; Buseck, P. R. Individual Aerosol Particles from Biomass Burning in Southern Africa: 2, Compositions and Aging of Inorganic Particles. *J. Geophys. Res.* **2003**, *108* (D13), 2002JD002310.
(16) Collier, S.; Zhou, S.; Onasch, T. B.; Jaffe, D. A.; Kleinman, L.; Sedlacek, A. J.; Briggs, N. L.; Hee, J.; Fortner, E.; Shilling, J. E.; et al. Regional Influence of Aerosol Emissions from Wildfires Driven by Combustion Efficiency: Insights from the BBOP Campaign. *Environ. Sci. Technol.* **2016**, *50* (16), 8613−8622.
(17) Decker, Z. C. J.; Zarzana, K. J.; Coggon, M.; Min, K.-E.; Pollack, I.; Ryerson, T. B.; Peischl, J.; Edwards, P.; Dubé, W. P.; Markovic, M. Z.; et al. Nighttime Chemical Transformation in Biomass Burning Plumes: A Box Model Analysis Initialized with Aircraft Observations. *Environ. Sci. Technol.* **2019**, *53* (5), 2529−2538.
(18) Decker, Z. C. J.; Robinson, M. A.; Barsanti, K. C.; Bourgeois, I.; Coggon, M. M.; DiGangi, J. P.; Diskin, G. S.; Flocke, F. M.; Franchin, A.; Fredrickson, C. D.; et al. Nighttime and Daytime Dark Oxidation Chemistry in Wildfire Plumes: An Observation and Model Analysis of FIREX-AQ Aircraft Data. *Atmos. Chem. Phys.* **2021**, *21* (21), 16293−16317.
(19) Hopkins, R. J.; Lewis, K.; Desyaterik, Y.; Wang, Z.; Tivanski, A. V.; Arnott, W. P.; Laskin, A.; Gilles, M. K. Correlations between Optical, Chemical and Physical Properties of Biomass Burn Aerosols. *Geophys. Res. Lett.* **2007**, *34* (18), L18806.
(20) Laskin, A.; Laskin, J.; Nizkorodov, S. A. Chemistry of Atmospheric Brown Carbon. *Chem. Rev.* **2015**, *115* (10), 4335−4382.
(21) Li, C.; Ma, Z.; Chen, J.; Wang, X.; Ye, X.; Wang, L.; Yang, X.; Kan, H.; Donaldson, D. J.; Mellouki, A. Evolution of Biomass Burning Smoke Particles in the Dark. *Atmos. Environ.* **2015**, *120*, 244−252.
(22) Pandey, A.; Shetty, N. J.; Chakrabarty, R. K. Aerosol Light Absorption from Optical Measurements of PTFE Membrane Filter Samples: Sensitivity Analysis of Optical Depth Measures. *Atmos. Meas. Technol.* **2019**, *12* (2), 1365−1373.
(23) Turco, R. P.; Yu, F. Aerosol Invariance in Expanding Coagulating Plumes. *Geophys. Res. Lett.* **1997**, *24* (10), 1223−1226.
(24) Turco, R. P.; Yu, F. Particle Size Distributions in an Expanding Plume Undergoing Simultaneous Coagulation and Condensation. *J. Geophys. Res.* **1999**, *104* (D16), 19227−19241.
(25) Sakamoto, K. M.; Laing, J. R.; Stevens, R. G.; Jaffe, D. A.; Pierce, J. R. The Evolution of Biomass-Burning Aerosol Size Distributions Due to Coagulation: Dependence on Fire and Meteorological Details and Parameterization. *Atmos. Chem. Phys.* **2016**, *16* (12), 7709−7724.
(26) Lee, K. W.; Chen, H. Coagulation Rate of Polydisperse Particles. *Aerosol Sci. Technol.* **1984**, *3* (3), 327−334.
(27) Reid, J. S.; Hobbs, P. V.; Ferek, R. J.; Blake, D. R.; Martins, J. V.; Dunlap, M. R.; Liousse, C. Physical, Chemical, and Optical Properties of Regional Hazes Dominated by Smoke in Brazil. *J. Geophys. Res.* **1998**, *103* (D24), 32059−32080.
(28) Abel, S. J.; Haywood, J. M.; Highwood, E. J.; Li, J.; Buseck, P. R. Evolution of Biomass Burning Aerosol Properties from an Agricultural Fire in Southern Africa. *Geophys. Res. Lett.* **2003**, *30* (15), 1783.
(29) Hennigan, C. J.; Westervelt, D. M.; Riipinen, I.; Engelhart, G. J.; Lee, T.; Collett, J. L.; Pandis, S. N.; Adams, P. J.; Robinson, A. L. New Particle Formation and Growth in Biomass Burning Plumes: An Important Source of Cloud Condensation Nuclei. *Geophys. Res. Lett.* **2012**, *39* (9), 2012GL050930.
(30) Adler, G.; Flores, J. M.; Abo Riziq, A.; Borrmann, S.; Rudich, Y. Chemical, Physical, and Optical Evolution of Biomass Burning Aerosols: A Case Study. *Atmos. Chem. Phys.* **2011**, *11* (4), 1491−1503.
(31) Jimenez, J. L.; Canagaratna, M. R.; Donahue, N. M.; Prevot, A. S. H.; Zhang, Q.; Kroll, J. H.; DeCarlo, P. F.; Allan, J. D.; Coe, H.; Ng, N. L.; et al. Evolution of Organic Aerosols in the Atmosphere. *Science* **2009**, *326* (5959), 1525−1529.
(32) Jolleys, M. D.; Coe, H.; McFiggans, G.; Taylor, J. W.; O'Shea, S. J.; Le Breton, M.; Bauguitte, S. J.-B.; Moller, S.; Di Carlo, P.; Aruffo, E.; Palmer, P. I.; et al. Properties and Evolution of Biomass Burning Organic Aerosol from Canadian Boreal Forest Fires. *Atmos. Chem. Phys.* **2015**, *15* (6), 3077−3095.
(33) Hodshire, A. L.; Akherati, A.; Alvarado, M. J.; Brown-Steiner, B.; Jathar, S. H.; Jimenez, J. L.; Kreidenweis, S. M.; Lonsdale, C. R.; Onasch, T. B.; Ortega, A. M.; et al. Aging Effects on Biomass Burning Aerosol Mass and Composition: A Critical Review of Field and Laboratory Studies. *Environ. Sci. Technol.* **2019**, *53* (17), 10007−10022.
(34) Tomlin, J. M.; Weis, J.; Veghte, D. P.; China, S.; Fraund, M.; He, Q.; Reicher, N.; Li, C.; Jankowski, K. A.; Rivera-Adorno, F. A.; et al. Chemical Composition and Morphological Analysis of Atmospheric Particles from an Intensive Bonfire Burning Festival. *Environ. Sci.: Atmos* **2022**, *2* (4), 616−633.
(35) Siemens, K. S. A.; Pagonis, D.; Guo, H.; Schueneman, M. K.; Dibb, J. E.; Campuzano-Jost, P.; Jimenez, J. L.; Laskin, A. Probing Atmospheric Aerosols by Multimodal Mass Spectrometry Techniques: Revealing Aging Characteristics of Its Individual Molecular Components. *ACS Earth Space Chem.* **2023**, *7* (12), 2498−2510.
(36) Semeniuk, T. A.; Wise, M. E.; Martin, S. T.; Russell, L. M.; Buseck, P. R. Hygroscopic Behavior of Aerosol Particles from Biomass Fires Using Environmental Transmission Electron Microscopy. *J. Atmos. Chem.* **2007**, *56* (3), 259−273.
(37) Carrico, C. M.; Petters, M. D.; Kreidenweis, S. M.; Sullivan, A. P.; McMeeking, G. R.; Levin, E. J. T.; Engling, G.; Malm, W. C.; Collett, J. L. Water Uptake and Chemical Composition of Fresh Aerosols Generated in Open Burning of Biomass. *Atmos. Chem. Phys.* **2010**, *10* (11), 5165−5178.
(38) Warneke, C.; Schwarz, J. P.; Dibb, J.; Kalashnikova, O.; Frost, G.; Al-Saad, J.; Brown, S. S.; Brewer, W. A.; Soja, A.; Seidel, F. C.; et al. The FIREX-AQ Science Team. Fire Influence on Regional to Global Environments and Air Quality (FIREX-AQ). *J. Geophys. Res.: Atmos* **2023**, *128* (2), No. e2022JD037758.
(39) Azzarello, L.; Washenfelder, R. A.; Robinson, M. A.; Franchin, A.; Womack, C. C.; Holmes, C. D.; Brown, S. S.; Middlebrook, A.; Newberger, T.; Sweeney, C.; et al. Characterization of Water-Soluble Brown Carbon Chromophores from Wildfire Plumes in the Western USA Using Size-Exclusion Chromatography. *Atmos. Chem. Phys.* **2023**, *23* (24), 15643−15654.
(40) Gkatzelis, G. I.; Coggon, M. M.; Stockwell, C. E.; Hornbrook, R. S.; Allen, H.; Apel, E. C.; Bela, M. M.; Blake, D. R.; Bourgeois, I.; Brown, S. S.; et al. Parameterizations of US Wildfire and Prescribed Fire Emission Ratios and Emission Factors Based on FIREX-AQ Aircraft Measurements. *Atmos. Chem. Phys.* **2024**, *24* (2), 929−956.
(41) Washenfelder, R. A.; Azzarello, L.; Ball, K.; Brown, S. S.; Decker, Z. C. J.; Franchin, A.; Fredrickson, C. D.; Hayden, K.; Holmes, C. D.; Middlebrook, A. M.; et al. Complexity in the Evolution, Composition, and Spectroscopy of Brown Carbon in Aircraft Measurements of Wildfire Plumes. *Geophys. Res. Lett.* **2022**, *49* (9), No. e2022GL098951.

https://doi.org/10.1021/acsearthspacechem.4c00215
ACS Earth Space Chem. XXXX, XXX, XXX−XXX

(42) *NASA Airborne Science Data for Atmospheric Composition*. https://www-air.larc.nasa.gov/cgi-bin/ArcView/firexaq?ANALYSIS=1. accessed 2024 July 23.
(43) Crosson, E. R. A Cavity Ring-down Analyzer for Measuring Atmospheric Levels of Methane, Carbon Dioxide, and Water Vapor. *Appl. Phys. B: lasers Opt.* **2008**, *92* (3), 403−408.
(44) Karion, A.; Sweeney, C.; Wolter, S.; Newberger, T.; Chen, H.; Andrews, A.; Kofler, J.; Neff, D.; Tans, P. Long-Term Greenhouse Gas Measurements from Aircraft. *Atmos. Meas. Technol.* **2013**, *6* (3), 511−526.
(45) DeCarlo, P. F.; Kimmel, J. R.; Trimborn, A.; Northway, M. J.; Jayne, J. T.; Aiken, A. C.; Gonin, M.; Fuhrer, K.; Horvath, T.; Docherty, K. S.; et al. Field-Deployable High-Resolution, Time-of-Flight Aerosol Mass Spectrometer. *Anal. Chem.* **2006**, *78* (24), 8281−8289.
(46) Liggio, J.; Li, S.-M.; Hayden, K.; Taha, Y. M.; Stroud, C.; Darlington, A.; Drollette, B. D.; Gordon, M.; Lee, P.; Liu, P.; et al. Oil Sands Operations as a Large Source of Secondary Organic Aerosols. *Nature* **2016**, *534* (7605), 91−94.
(47) Rickly, P. S.; Guo, H.; Campuzano-Jost, P.; Jimenez, J. L.; Wolfe, G. M.; Bennett, R.; Bourgeois, I.; Crounse, J. D.; Dibb, J. E.; DiGangi, J. P.; et al. Emission Factors and Evolution of SO_2 Measured from Biomass Burning in Wildfires and Agricultural Fires. *Atmos. Chem. Phys.* **2022**, *22* (23), 15603−15620.
(48) Canagaratna, M. R.; Jimenez, J. L.; Kroll, J. H.; Chen, Q.; Kessler, S. H.; Massoli, P.; Hildebrandt Ruiz, L.; Fortner, E.; Williams, L. R.; Wilson, K. R.; et al. Elemental Ratio Measurements of Organic Compounds Using Aerosol Mass Spectrometry: Characterization, Improved Calibration, and Implications. *Atmos. Chem. Phys.* **2015**, *15* (1), 253−272.
(49) Kroll, J. H.; Donahue, N. M.; Jimenez, J. L.; Kessler, S. H.; Canagaratna, M. R.; Wilson, K. R.; Altieri, K. E.; Mazzoleni, L. R.; Wozniak, A. S.; Bluhm, H.; et al. Carbon Oxidation State as a Metric for Describing the Chemistry of Atmospheric Organic Aerosol. *Nat. Chem.* **2011**, *3* (2), 133−139.
(50) Lee, B. H.; Lopez-Hilfiker, F. D.; Mohr, C.; Kurtén, T.; Worsnop, D. R.; Thornton, J. A. An Iodide-Adduct High-Resolution Time-of-Flight Chemical-Ionization Mass Spectrometer: Application to Atmospheric Inorganic and Organic Compounds. *Environ. Sci. Technol.* **2014**, *48* (11), 6309−6317.
(51) Palm, B. B.; Liu, X.; Jimenez, J. L.; Thornton, J. A. Performance of a New Coaxial Ion−Molecule Reaction Region for Low-Pressure Chemical Ionization Mass Spectrometry with Reduced Instrument Wall Interactions. *Atmos. Meas. Technol.* **2019**, *12* (11), 5829−5844.
(52) Zeng, L.; Sullivan, A. P.; Washenfelder, R. A.; Dibb, J.; Scheuer, E.; Campos, T. L.; Katich, J. M.; Levin, E.; Robinson, M. A.; Weber, R. J. Assessment of Online Water-Soluble Brown Carbon Measuring Systems for Aircraft Sampling. *Atmos. Meas. Technol.* **2021**, *14* (10), 6357−6378.
(53) Liu, C.; Chung, C. E.; Yin, Y.; Schnaiter, M. The Absorption Ångström Exponent of Black Carbon: From Numerical Aspects. *Atmos. Chem. Phys.* **2018**, *18* (9), 6259−6273.
(54) Akagi, S. K.; Craven, J. S.; Taylor, J. W.; McMeeking, G. R.; Yokelson, R. J.; Burling, I. R.; Urbanski, S. P.; Wold, C. E.; Seinfeld, J. H.; Coe, H.; et al. Evolution of Trace Gases and Particles Emitted by a Chaparral Fire in California. *Atmos. Chem. Phys.* **2012**, *12* (3), 1397−1421.
(55) Vakkari, V.; Beukes, J. P.; Dal Maso, M.; Aurela, M.; Josipovic, M.; Van Zyl, P. G. Major Secondary Aerosol Formation in Southern African Open Biomass Burning Plumes. *Nat. Geosci.* **2018**, *11* (8), 580−583.
(56) He, Y.; Zhao, B.; Wang, S.; Valorso, R.; Chang, X.; Yin, D.; Feng, B.; Camredon, M.; Aumont, B.; Dearden, A.; et al. Formation of Secondary Organic Aerosol from Wildfire Emissions Enhanced by Long-Time Ageing. *Nat. Geosci.* **2024**, *17* (2), 124−129.
(57) Kodros, J. K.; Papanastasiou, D. K.; Paglione, M.; Masiol, M.; Squizzato, S.; Florou, K.; Skyllakou, K.; Kaltsonoudis, C.; Nenes, A.; Pandis, S. N. Rapid Dark Aging of Biomass Burning as an Overlooked Source of Oxidized Organic Aerosol. *Proc. Natl. Acad. Sci. U.S.A.* **2020**, *117* (52), 33028−33033.
(58) Robinson, M. A.; Decker, Z. C. J.; Barsanti, K. C.; Coggon, M. M.; Flocke, F. M.; Franchin, A.; Fredrickson, C. D.; Gilman, J. B.; Gkatzelis, G. I.; Holmes, C. D.; et al. Variability and Time of Day Dependence of Ozone Photochemistry in Western Wildfire Plumes. *Environ. Sci. Technol.* **2021**, *55* (15), 10280−10290.
(59) May, A. A.; Lee, T.; McMeeking, G. R.; Akagi, S.; Sullivan, A. P.; Urbanski, S.; Yokelson, R. J.; Kreidenweis, S. M. Observations and Analysis of Organic Aerosol Evolution in Some Prescribed Fire Smoke Plumes. *Atmos. Chem. Phys.* **2015**, *15* (11), 6323−6335.
(60) Adachi, K.; Sedlacek, A. J.; Kleinman, L.; Springston, S. R.; Wang, J.; Chand, D.; Hubbe, J. M.; Shilling, J. E.; Onasch, T. B.; Kinase, T.; et al. Spherical Tarball Particles Form through Rapid Chemical and Physical Changes of Organic Matter in Biomass-Burning Smoke. *Proc. Natl. Acad. Sci. U.S.A.* **2019**, *116* (39), 19336−19341.
(61) Pagonis, D.; Selimovic, V.; Campuzano-Jost, P.; Guo, H.; Day, D. A.; Schueneman, M. K.; Nault, B. A.; Coggon, M. M.; DiGangi, J. P.; Diskin, G. S.; et al. Impact of Biomass Burning Organic Aerosol Volatility on Smoke Concentrations Downwind of Fires. *Environ. Sci. Technol.* **2023**, *57* (44), 17011−17021.
(62) Mathai, S.; Veghte, D.; Kovarik, L.; Mazzoleni, C.; Tseng, K.-P.; Bucci, S.; Capek, T.; Cheng, Z.; Marinoni, A.; China, S. Optical Properties of Individual Tar Balls in the Free Troposphere. *Environ. Sci. Technol.* **2023**, *57* (44), 16834−16842.
(63) Lin, P.; Aiona, P. K.; Li, Y.; Shiraiwa, M.; Laskin, J.; Nizkorodov, S. A.; Laskin, A. Molecular Characterization of Brown Carbon in Biomass Burning Aerosol Particles. *Environ. Sci. Technol.* **2016**, *50* (21), 11815−11824.
(64) Palm, B. B.; Peng, Q.; Fredrickson, C. D.; Lee, B. H.; Garofalo, L. A.; Pothier, M. A.; Kreidenweis, S. M.; Farmer, D. K.; Pokhrel, R. P.; Shen, Y.; et al. Quantification of Organic Aerosol and Brown Carbon Evolution in Fresh Wildfire Plumes. *Proc. Natl. Acad. Sci. U.S.A.* **2020**, *117* (47), 29469−29477.
(65) Fredrickson, C. D.; Palm, B. B.; Lee, B. H.; Zhang, X.; Orlando, J. J.; Tyndall, G. S.; Garofalo, L. A.; Pothier, M. A.; Farmer, D. K.; Decker, Z. C. J.; et al. Formation and Evolution of Catechol-Derived SOA Mass, Composition, Volatility, and Light Absorption. *ACS Earth Space Chem.* **2022**, *6* (4), 1067−1079.
(66) Hand, J. L.; Day, D. E.; McMeeking, G. M.; Levin, E. J. T.; Carrico, C. M.; Kreidenweis, S. M.; Malm, W. C.; Laskin, A.; Desyaterik, Y. Measured and Modeled Humidification Factors of Fresh Smoke Particles from Biomass Burning: Role of Inorganic Constituents. *Atmos. Chem. Phys.* **2010**, *10* (13), 6179−6194.
(67) Lewis, K. A.; Arnott, W. P.; Malm, W. C.; Laskin, A.; Jimenez, J. L.; Ulbrich, I. M.; Huffman, J. A.; Onasch, T. B.; Trimborn, A.; Liu, L.; et al. Reduction in Biomass Burning Aerosol Light Absorption upon Humidification: Roles of Inorganically-Induced Hygroscopicity, Particle Collapse, and Photoacoustic Heat and Mass Transfer. *Atmos. Chem. Phys.* **2009**, *9*, 8949−8966.
(68) Takegawa, N.; Miyazaki, Y.; Kondo, Y.; Komazaki, Y.; Miyakawa, T.; Jimenez, J. L.; Jayne, J. T.; Worsnop, D. R.; Allan, J. D.; Weber, R. J. Characterization of an Aerodyne Aerosol Mass Spectrometer (AMS): Intercomparison with Other Aerosol Instruments. *Aerosol Sci. Technol.* **2005**, *39* (8), 760−770.
(69) Trebs, I.; Metzger, S.; Meixner, F. X.; Helas, G.; Hoffer, A.; Rudich, Y.; Falkovich, A. H.; Moura, M. A. L.; Da Silva, R. S.; Artaxo, P.; et al. The NH_4^+-NO_3^--Cl^--SO_4^{2-}-H_2O Aerosol System and Its Gas Phase Precursors at a Pasture Site in the Amazon Basin: How Relevant Are Mineral Cations and Soluble Organic Acids? *J. Geophys. Res.* **2005**, *110* (D7), 2004JD005478.
(70) Wexler, A. S.; Clegg, S. L. Atmospheric Aerosol Models for Systems Including the Ions H^+, NH_4^+, Na^+, SO_4^{2-}, NO_3^-, Cl^-, Br^-, and H_2O. *J. Geophys. Res.* **2002**, *107* (D14), ACH 14−1-ACH 14-14.
(71) Guo, H.; Liu, J.; Froyd, K. D.; Roberts, J. M.; Veres, P. R.; Hayes, P. L.; Jimenez, J. L.; Nenes, A.; Weber, R. J. Fine Particle pH and Gas−Particle Phase Partitioning of Inorganic Species in Pasadena,

https://doi.org/10.1021/acsearthspacechem.4c00215
ACS Earth Space Chem. XXXX, XXX, XXX−XXX

California, during the 2010 CalNex Campaign. *Atmos. Chem. Phys.* **2017**, *17* (9), 5703−5719.
(72) Cadle, S. H.; Countess, R. J.; Kelly, N. A. Nitric Acid and Ammonia in Urban and Rural Locations. *Atmos. Environ.* **1982**, *16* (10), 2501−2506.
(73) Watson, J. G.; Chow, J. C.; Lurmann, F. W.; Musarra, S. P. Ammonium Nitrate Nitric Acid, and Ammonia Equilibrium in Wintertime Phoenix, Arizona. *Air Waste* **1994**, *44* (4), 405−412.
(74) Rivera-Adorno, F. A.; Tomlin, J. M.; Lata, N. N.; Azzarello, L.; Robinson, M. A.; Washenfelder, R. A.; Franchin, A.; Middlebrook, A. M.; China, S.; Brown, S. S.; Young, C. J.; Fraund, M.; Moffet, R. C.; Laskin, A. Chemical Imaging of Atmospheric Biomass Burning Particles from North American Wildfires. *ACS ES&T Air* **2024**.
(75) Behera, S. N.; Balasubramanian, R. Influence of Biomass Burning on Temporal and Diurnal Variations of Acidic Gases, Particulate Nitrate, and Sulfate in a Tropical Urban Atmosphere. *Adv. Meteorol.* **2014**, *2014*, 1−13.
(76) Liu, T.; Chan, A. W. H.; Abbatt, J. P. D. Multiphase Oxidation of Sulfur Dioxide in Aerosol Particles: Implications for Sulfate Formation in Polluted Environments. *Environ. Sci. Technol.* **2021**, *55* (8), 4227−4242.
(77) Pio, C. A.; Harrison, R. M. Vapour Pressure of Ammonium Chloride Aerosol: Effect of Temperature and Humidity. *Atmos. Environ.* **1987**, *21* (12), 2711−2715.
(78) Laskin, A.; Moffet, R. C.; Gilles, M. K.; Fast, J. D.; Zaveri, R. A.; Wang, B.; Nigge, P.; Shutthanandan, J. Tropospheric Chemistry of Internally Mixed Sea Salt and Organic Particles: Surprising Reactivity of NaCl with Weak Organic Acids. *J. Geophys. Res.* **2012**, *117* (D15), 2012JD017743.
(79) Decker, Z. C. J.; Novak, G. A.; Aikin, K.; Veres, P. R.; Neuman, J. A.; Bourgeois, I.; Bui, T. P.; Campuzano-Jost, P.; Coggon, M. M.; Day, D. A.; et al. Airborne Observations Constrain Heterogeneous Nitrogen and Halogen Chemistry on Tropospheric and Stratospheric Biomass Burning Aerosol. *Geophys. Res. Lett.* **2024**, *51* (4), No. e2023GL107273.
(80) Ahern, A. T.; Goldberger, L.; Jahl, L.; Thornton, J.; Sullivan, R. C. Production of N_2O_5 and $ClNO_2$ through Nocturnal Processing of Biomass-Burning Aerosol. *Environ. Sci. Technol.* **2018**, *52* (2), 550−559.

https://doi.org/10.1021/acsearthspacechem.4c00215
ACS Earth Space Chem. XXXX, XXX, XXX−XXX